*International Journal of Microwave and Wireless Technologies*

**cambridge.org/mrf**

# The efficient implementation of IE-FFT algorithm with combined field integral equation for solving electromagnetic scattering problems

Seung Mo Seo

Agency for Defense Development, Daejeon, Korea

**Research Paper**

**Cite this article:** Seo SM (2021). The efficient implementation of IE-FFT algorithm with combined field integral equation for solving electromagnetic scattering problems. *International Journal of Microwave and Wireless Technologies* **13**, 137–143. https://doi.org/10.1017/S1759078720000653

Received: 30 November 2019
Revised: 27 April 2020
Accepted: 1 May 2020
First published online: 1 June 2020

**Key words:**
Combined field integral equation; fast Fourier transform; integral equation; method of moments

**Author for correspondence:**
Seung Mo Seo,
E-mail: seungmos@gmail.com

**Abstract**

An integral equation-fast Fourier transform (IE-FFT) algorithm is applied to the electromagnetic solutions of the combined field integral equation (CFIE) for scattering problems by an arbitrary-shaped three-dimensional perfect electric conducting object. The IE-FFT with CFIE uses a Cartesian grid for known Green's function to considerably reduce memory storage and speed up CPU time for both matrix fill-in and matrix vector multiplication when used with a generalized minimal residual method. The uniform interpolation of the Green's function on an equally spaced Cartesian grid allows a global FFT for field interaction terms. However, the near interaction terms do not take care for the singularity of the Green's function and should be adequately corrected. The IE-FFT with CFIE does not always require a suitable preconditioner for electrically large problems. It is shown that the complexity of the IE-FFT with CFIE is found to be approximately $O(N^{1.5})$ and $O(N^{1.5}\log N)$ for memory and CPU time, respectively.

## Introduction

The method of moments (MoM) [1] solutions of surface integral equations have been demonstrated to be very effective in analyzing the electromagnetic (EM) radiation and scattering problems. The electric field integral equation (EFIE), the magnetic field integral equation (MFIE), and the combined field integral equation (CFIE) have been popular choices for an arbitrary three-dimensional (3-D) perfect electric conducting (PEC) object. However, conventional MoM solutions suffer from $O(N^2)$ storage for matrix fill-in and $O(N^2)$ operations per iteration for matrix vector multiplication (MVM) with an iterative matrix solver. Both the EFIE and the MFIE suffer from the interior resonance problem. To overcome these difficulties, this paper proposes an integral equation-fast Fourier transform (IE-FFT) algorithm with CFIE as the extension of the IE-FFT algorithm [2] without the help of a preconditioner. The conventional IE-FFT with EFIE should have a preconditioner for electrically large structures.

One of the fastest and most efficient algorithms for the MoM solutions is the multilevel fast multipole method [3], which reduces the computational complexity from $O(N^2)$ to $O(N\log N)$. Unfortunately, the strong dependence of multipole-based methods on integral kernels makes the methods inadequate for general kernel-independent techniques. To avoid the kernel-dependence, algebraically mathematical algorithms such as integral equation-QR factorization [4] and adaptive cross approximation (ACA) [5] have been proposed. Nevertheless, the numerical complexity of these algorithms may not be clear whether it is $O(N^{1.5})$ or not.

There is another physical class of fast IE methods based on grid-based approaches such as the adaptive integral method (AIM) [6], the precorrected-FFT (p-FFT) [7, 8], and the IE-FFT. The AIM and the p-FFT algorithms need unknown "equivalent" source approximation on a Cartesian grid. Unlike these algorithms, the IE-FFT applies known Green's function interpolation on a Cartesian grid. The IE-FFT algorithm uses one global FFT for field interaction terms [2, 9]. However, the near-field interaction terms do not take care of the singularity of the Green's function and are adequately corrected by the traditional MoM. Recently, a couple of the IE-FFT papers with CFIE [10, 11] have been published. One IE-FFT with CFIE [10] is to use the gradient of Rao–Wilton–Glisson (RWG) basis function. The weakness of the paper should have the second order of the RWG basis function to obtain the same order of accuracy with the conventional MoM. To overcome this problem, another IE-FFT with CFIE [11] is proposed. However, the paper uses two coefficient matrices of Green's function, which is the most dominant numerical complexity in the IE-FFT. The proposed IE-FFT algorithm with CFIE follows the basic guidelines from the original IE-FFT paper [2]. The uniqueness of the IE-FFT algorithm lies on the simplicity and the rigorous error control. The Lagrange interpolation of Green's function simplifies the formulation and enables an efficient algorithmic implementation. The proposed IE-FFT algorithm with CFIE not only has better convergence rate but also removes the interior resonance. The IE-FFT with CFIE does not always

© Cambridge University Press and the European Microwave Association 2020

CAMBRIDGE UNIVERSITY PRESS

need to have an appropriate preconditioner. Also, it works algebraically simple Lagrange polynomials on a 3-D uniform Cartesian grid. The proposed algorithm definitely guarantees $O(N^{1.5})$ complexity for memory requirement and $O(N^{1.5}\log N)$ complexity for MVM.

## CFIE formulation

The CFIE formulation is well known for an arbitrarily shaped 3-D PEC objects. The resulting matrix equation can be written as

$$Z^{CFIE} \cdot J = V^{CFIE}, \tag{1}$$

where $Z^{CFIE}$ is the impedance matrix, $J$ is the unknown surface current vector, and $V^{CFIE}$ is right-hand side (RHS) vector. The impedance matrix is rewritten as

$$Z^{CFIE} = \rho Z^{EFIE} + \eta_0(1-\rho)Z^{MFIE}, \tag{2}$$

where $\rho$ is the weighting constant of the CFIE and $\eta_0$ is the intrinsic impedance of free space. The entries of the impedance matrices $Z^{EFIE}$ and $Z^{MFIE}$ for the EFIE and the MFIE are, respectively, given by

$$\begin{aligned} Z_{i,j}^{EFIE} &= k_0^2 A_{i,j} - D_{i,j} \\ Z_{i,j}^{MFIE} &= \frac{1}{2}C_{i,j} - P_{i,j} \end{aligned} \qquad 0 \le i,j \le N-1, \tag{3}$$

where

$$A_{i,j} = \int\limits_{supp(\vec{\alpha}_i)} \vec{\alpha}_i(\vec{r}) \cdot \int\limits_{supp(\vec{\alpha}_j)} g(\vec{r};\vec{r}\,')\vec{\alpha}_j(\vec{r}\,')d\Gamma' d\Gamma, \tag{4}$$

$$D_{i,j} = \int\limits_{supp(\vec{\alpha}_i)} div_\Gamma \vec{\alpha}_i(\vec{r}) \int\limits_{supp(\vec{\alpha}_j)} g(\vec{r};\vec{r}\,')div'_\Gamma \vec{\alpha}_j(\vec{r}\,')d\Gamma' d\Gamma, \tag{5}$$

$$C_{i,j} = \int\limits_{supp(\vec{\alpha}_i)} \vec{\alpha}_i(\vec{r}) \cdot \vec{\alpha}_j(\vec{r})d\Gamma, \tag{6}$$

and

$$P_{i,j} = \int\limits_{supp(\vec{\alpha}_i)} (\vec{\alpha}_i(\vec{r}) \times \hat{n}_i) \cdot \int\limits_{supp(\vec{\alpha}_j)} \vec{\alpha}_j(\vec{r}\,') \times \nabla' g(\vec{r};\vec{r}\,')d\Gamma' d\Gamma. \tag{7}$$

$N$ is the number of unknowns. Note that $supp()$ indicates the support of non-boundary edge. Here, $\mathbf{A}_{i,j}$ and $\mathbf{D}_{i,j}$ are the impedance entries of vector and scalar potentials from the discrete Galerkin statement of the EFIE. $\mathbf{C}_{i,j}$ and $\mathbf{P}_{i,j}$ are singular and coupling entries of the impedance matrix from the discrete Galerkin statement of the MFIE. In the paper, the free-space Green's function $g(\vec{r};\vec{r}\,') = e^{-jk_0|\vec{r}-\vec{r}\,'|}/|\vec{r}-\vec{r}\,'|$ is considered. The free-space wave number is denoted by $k_0$. $\vec{\alpha}_i(\vec{r})$ stands for surface div-conforming vector RWG basis function [12]. The RHS is given by

$$V^{CFIE} = \rho V^{EFIE} + \eta_0(1-\rho)V^{MFIE}. \tag{8}$$

The entries of the RHS vector are written as

$$V_i^{EFIE} = -4\pi \frac{jk_0}{\eta_0} \int\limits_{supp(\vec{\alpha}_i)} \vec{\alpha}_i(\vec{r}) \cdot \vec{E}^{inc}(\vec{r})d\Gamma \tag{9}$$

and

$$V_i^{MFIE} = 4\pi \int\limits_{supp(\vec{\alpha}_i)} \vec{\alpha}_i(r) \cdot [\hat{n} \times \vec{H}^{inc}(\vec{r})]d\Gamma \tag{10}$$

where $\vec{E}^{inc}(\vec{r})$ and $\vec{H}^{inc}(\vec{r})$ are the incident electric and magnetic field intensities, respectively.

## The IE-FFT algorithm with CFIE

The IE-FFT algorithm with CFIE constructs a 3-D hexahedron bounding box that encloses the entire geometry. Figure 1 shows two discretizations: a triangular mesh for unknown RWG basis functions and a uniform Cartesian grid for known free-space Green's function.

Note that $C_{NF}$ is a constant used to define the near-field correction region, and $\lambda_0$ is the wavelength in free space. Note $r_L$ is the sampling resolution. For example, $L$ is the size of the third-order Cartesian element, which is the 3-D tensor product form of 1-D piecewise Lagrange polynomials on a Cartesian grid. The free-space Green's function can be written as

$$\begin{aligned} g(\vec{r};\vec{r}\,') &= \frac{e^{-jk_0R}}{R} = \frac{e^{-jk_0|\vec{r}-\vec{r}\,'|}}{|\vec{r}-\vec{r}\,'|} \\ &\simeq \sum_n \sum_{n'} \beta_n^p(\vec{r}) g_{n,n'} \beta_{n'}^p(\vec{r}\,') \end{aligned} \qquad 0 \le n,n' \le N_g - 1, \tag{11}$$

where $p$ is the order of Lagrange polynomials and $N_g$ is the number of 3-D Cartesian grid points. $\beta_n^p(\vec{r})$ is the $p^{\text{th}}$-order Lagrange interpolation basis function and $g_{n,n'}$ is the "known" coefficient of the free-space Green's function. The vector and matrix form of the free-space Green's function can be expressed as

$$g(\vec{r};\vec{r}\,') \simeq \beta(\vec{r}) \cdot G \cdot \beta^T(\vec{r}\,'), \tag{12}$$

where

$$\beta(\vec{r}) = \begin{bmatrix} \beta_0^p(x)\beta_0^p(y)\beta_0^p(z) \\ \beta_1^p(x)\beta_0^p(y)\beta_0^p(z) \\ \vdots \\ \beta_{N_x-1}^p(x)\beta_{N_y-1}^p(y)\beta_{N_z-1}^p(z) \end{bmatrix}^T \tag{13}$$

and

$$G = \begin{bmatrix} g_{0,0} & g_{0,1} & \cdots & g_{0,N_g-1} \\ g_{1,0} & g_{1,1} & \cdots & g_{1,N_g-1} \\ \vdots & \vdots & \ddots & \vdots \\ g_{N_g-1,0} & g_{N_g-1,1} & \cdots & g_{N_g-1,N_g-1} \end{bmatrix}. \tag{14}$$

https://doi.org/10.1017/S1759078720000653 Published online by Cambridge University Press

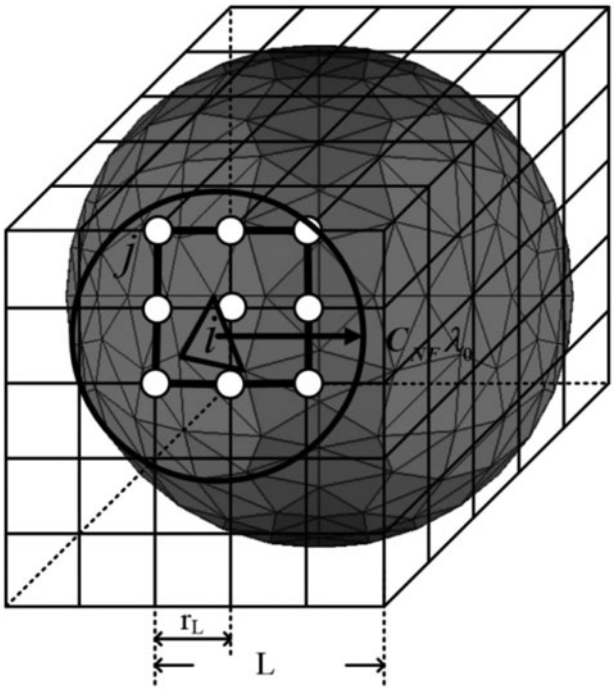



**Fig. 1.** Two discretizations for unknown surface current density and known free-space Green's function.

Equation (3) is combined with equation (11) as follows:

$$\begin{aligned} Z_{IE-FFT}^{EFIE} &= k_0^2 \vec{\Pi}_A \cdot G \cdot (\vec{\Pi}_A)^T - \Pi_D \cdot G \cdot (\Pi_D)^T \\ Z_{IE-FFT}^{MFIE} &= \frac{1}{2} C - \vec{\Pi}_N \cdot G \cdot (\vec{\Pi}_P)^T, \end{aligned} \tag{15}$$

where

$$\vec{\Pi}_A = \int_\Gamma \begin{bmatrix} \vec{\alpha}_0(\vec{r}) \\ \vec{\alpha}_1(\vec{r}) \\ \vdots \\ \vec{\alpha}_{N-1}(\vec{r}) \end{bmatrix} \begin{bmatrix} \beta_0^p(\vec{r}) & \beta_1^p(\vec{r}) & \cdots & \beta_{N_g-1}^p(\vec{r}) \end{bmatrix} d\Gamma, \tag{16}$$

$$\Pi_D = \int_\Gamma \begin{bmatrix} div_\Gamma \vec{\alpha}_0(\vec{r}) \\ div_\Gamma \vec{\alpha}_1(\vec{r}) \\ \vdots \\ div_\Gamma \vec{\alpha}_{N-1}(\vec{r}) \end{bmatrix} \begin{bmatrix} \beta_0^p(\vec{r}) & \beta_1^p(\vec{r}) & \cdots & \beta_{N_g-1}^p(\vec{r}) \end{bmatrix} d\Gamma, \tag{17}$$

$$\vec{\Pi}_N = \int_\Gamma \begin{bmatrix} \vec{\alpha}_0(\vec{r}) \times \hat{n}_0 \\ \vec{\alpha}_1(\vec{r}) \times \hat{n}_1 \\ \vdots \\ \vec{\alpha}_{N-1}(\vec{r}) \times \hat{n}_{N-1} \end{bmatrix} \begin{bmatrix} \beta_0^p(\vec{r}) & \beta_1^p(\vec{r}) & \cdots & \beta_{N_g-1}^p(\vec{r}) \end{bmatrix} d\Gamma, \tag{18}$$

and

$$\vec{\Pi}_P = \int_\Gamma \begin{bmatrix} \vec{\alpha}_0(\vec{r}) \\ \vec{\alpha}_1(\vec{r}) \\ \vdots \\ \vec{\alpha}_{N-1}(\vec{r}) \end{bmatrix} \times \begin{bmatrix} \nabla\beta_0^p(\vec{r}) & \nabla\beta_1^p(\vec{r}) & \cdots & \nabla\beta_{N_g-1}^p(\vec{r}) \end{bmatrix} d\Gamma. \tag{19}$$

The IE-FFT algorithm with CFIE has three vector and one scalar $\mathbf{\Pi}$ matrices. One vector and one scalar matrix come from the EFIE and the other two vectors from the MFIE. When an iterative solver is used, the near- and far-field computations of the IE-FFT algorithm with CFIE are described below. $d$ indicates the distance between basis and testing functions.

### *Near-field computation* ($d \le C_{NF}\lambda_0$)

From equation (1), the MVM is computed by

$$y = Z^{CFIE} \cdot x. \tag{20}$$

The matrix $Z^{CFIE}$ is obtained by the traditional MoM approach.

### *Far-field computation* ($d > C_{NF}\lambda_0$)

From equation (15), the MVM is performed by

$$\begin{aligned} y =& Z^{corr} \cdot x \\ &+ \rho \left\{ \begin{matrix} k_0^2 \vec{\Pi}_A \cdot IFFT[FFT(G) \cdot FFT((\vec{\Pi}_A)^T \cdot x)] \\ -\Pi_D \cdot IFFT[FFT(G) \cdot FFT((\Pi_D)^T \cdot x)] \end{matrix} \right\} \\ &- (1-\rho)\{\eta_0 \vec{\Pi}_N \cdot IFFT[FFT(G) \cdot FFT((\vec{\Pi}_P)^T \cdot x)]\}, \end{aligned} \tag{21}$$

where $Z^{corr}$ is a correction matrix. In Fig. 1, the coupling between near-interaction terms separated at least by $C_{NF}\lambda_0$ should be sufficiently corrected to assure the accuracy. The coefficient of Green's function has singularity when a source and an observation point are close to each other. In this paper, $C_{NF}$ is chosen to be 0.3. The correction entries are given by

$$\begin{aligned} Z_{i,j}^{corr} =& Z_{i,j}^{CFIE} - \rho[k_0^2 (\vec{\Pi}_A)_{i,I} G_{I,J} (\vec{\Pi}_A)_{J,j}^T - (\Pi_D)_{i,I} G_{I,J} (\Pi_D)_{J,j}^T] \\ &+ (1-\rho)[(\vec{\Pi}_N)_{i,I} G_{I,J} (\vec{\Pi}_P)_{J,j}^T], \end{aligned} \tag{22}$$

where $0 \le i < N$, $j \in C_{neig}$, and $C_{neig}$ is the set of the near-field interaction elements within $C_{NF}\lambda_0$. The near-field terms between RWG basis functions $i$ and $j$ should be substituted by the entries of the traditional MoM techniques. The complexity of $Z^{corr}$ and $\mathbf{\Pi}$ matrices is $O(N)$. However, the dense $G$ matrix for the coefficients of Green's function leads to $O(N^3)$ storage and MVM per iteration for a Cartesian grid. By virtue of the FFT [13], the memory requirement reduces to $O(N^{1.5})$ and the MVM could be speeded up to $O(N^{1.5}\log N)$.

## Numerical results

To demonstrate the accuracy and efficiency of the proposed algorithm, a PEC sphere of 1 m is considered. The discretization of

https://doi.org/10.1017/S1759078720000653 Published online by Cambridge University Press

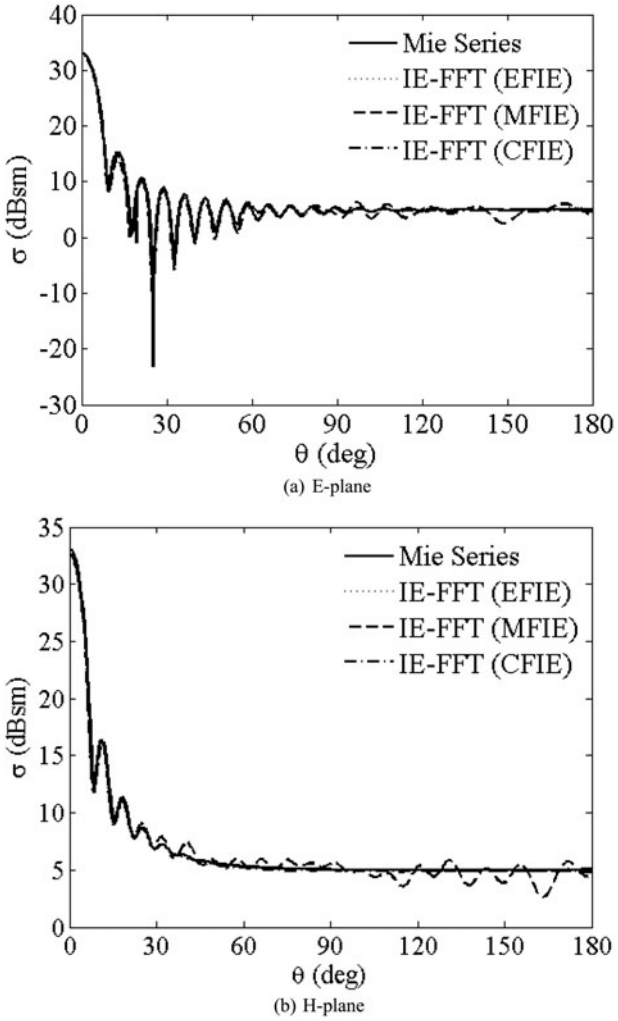



**Fig. 2.** Bistatic RCS results for 1 m PEC sphere at a frequency of 1200 MHz. (a) *E*-plane, (b) *H*-plane.

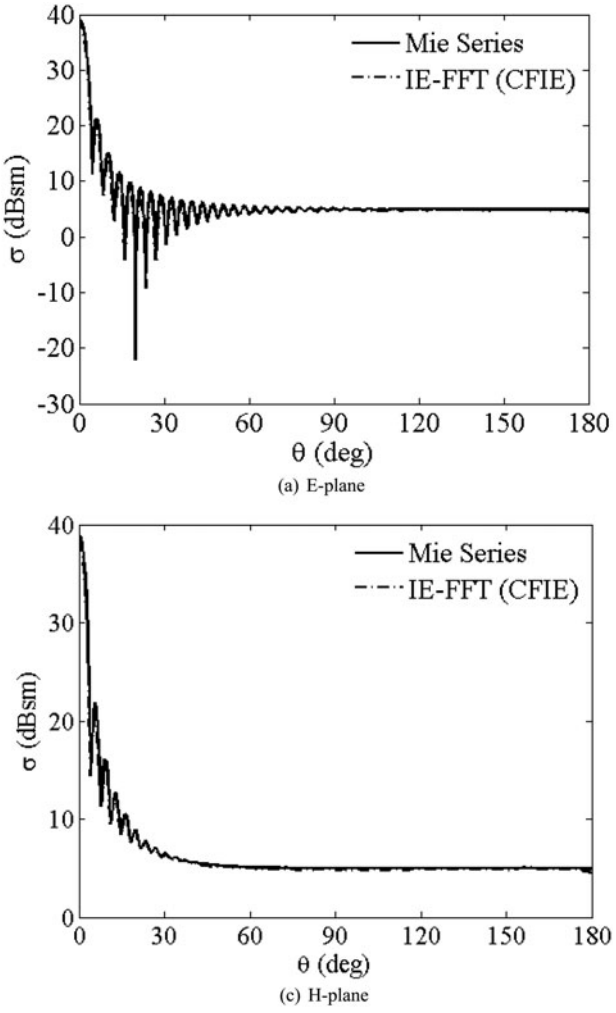



**Fig. 3.** Bistatic RCS results for 1 m PEC sphere at a frequency of 2400 MHz. (a) *E*-plane, (b) *H*-plane.

the triangular mesh is 7 elements per wavelength. All numerical simulations are carried out on a 2GB RAM Intel(R) Pentium(R) M processor 1.6 GHz. All computations have been done in single precision arithmetic. As a matrix solver, a generalized minimal residual (GMRES) method [14] is used without the help of any preconditioner. The residual tolerance is set to $1.0e-3$. In the simulation, the constant $\rho$ of the CFIE is chosen to be 0.5. Third-order Lagrange polynomials are used to interpolate free-space Green's function. Figure 2 shows the results of bistatic RCS at a frequency of 1200 MHz.

The IE-FFT with CFIE solution is compared with the analytic Mie series solution. Also, it is compared with the EFIE and the MFIE solutions accelerated by IE-FFT. The results of the IE-FFT with CFIE have very good agreements with those of Mie series at both *E*-plane and *H*-plane. The results of the EFIE also have good agreements but bad convergence rate. Despite good convergence, the results of the MFIE have some discrepancies when compared with those of the Mie series. As we have already known, the inaccuracy of the MFIE comes from the hyper-singular integration. Therefore, the EFIE has more accurate results than the CFIE, which has the weighting portion of the MFIE. The results of bistatic RCS at a frequency of 2400 MHz are shown in Fig. 3.

**Table 1.** Memory requirement of IE-FFT algorithm with CFIE for scattering from a PEC sphere with a radius of 1 m

| Frequency (MHz) | Unknowns | $Z^{corr}$ (MB) | Π (MB) | *G* (MB) |
|---|---|---|---|---|
| 300 | 3072 | 5.90 | 10.66 | 0.26 |
| 600 | 12 288 | 24.39 | 42.79 | 2.10 |
| 1200 | 49 152 | 98.29 | 169.21 | 16.78 |
| 2400 | 196 608 | 394.30 | 685 | 134.22 |

The IE-FFT of the EFIE does not converge within the number of iterations exceeded to a maximum of 2000. However, the IE-FFT with CFIE has a very good convergence rate and also accurate results at both *E*- and *H*-planes. Table 1 summarizes the performance of the IE-FFT algorithm with CFIE for third-order Lagrange polynomials in terms of memory. All units are megabytes (MB). The complexity of $Z^{corr}$ and Π matrices is clearly shown as $O(N)$. However, the complexity of *G* matrix is $O(N^{1.5})$.

https://doi.org/10.1017/S1759078720000653 Published online by Cambridge University Press

**Table 2.** CPU time and the number of iterations of IE-FFT algorithm with CFIE for scattering from a PEC sphere with a radius of 1 m

| | | | | Number of iterations | | |
|---|---|---|---|---|---|---|
| Frequency (MHz) | $Z^{corr}$ (s) | $\Pi$ (s) | MVM/iteration (s) | EFIE | MFIE | CFIE |
| 300 | 42 | 1 | 0.13 | 111 | 19 | 19 |
| 600 | 181 | 5 | 0.8 | 361 | 42 | 22 |
| 1200 | 699 | 20 | 4.29 | 1078 | 65 | 23 |
| 2400 | 2866 | 81 | 30.14 | >2000 | 282 | 25 |

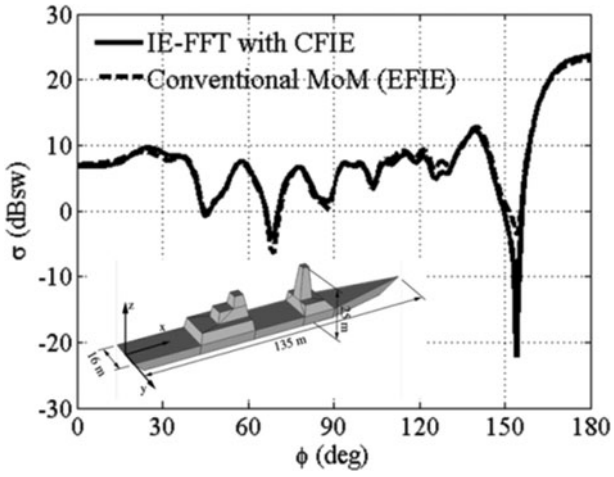



**Fig. 4.** Comparison of the bistatic RCS results for the battleship at 30 MHz ($\theta\theta$-polarization) using the IE-FFT with CFIE and the traditional MoM.

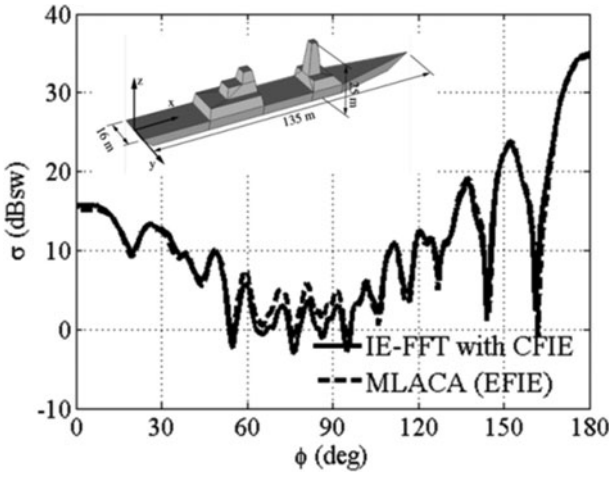



**Fig. 5.** Comparison of the bistatic RCS results for the battleship at 60 MHz ($\theta\theta$-polarization) using the IE-FFT with CFIE and the ACA algorithms.

Table 2 summarizes the CPU time and the number of iterations of the IE-FFT algorithm with CFIE. All units are seconds (sec). The number of iterations for the EFIE, MFIE, and the CFIE is tabularized in order. In a frequency of 2400 MHz, the EFIE does not converge within the number of iterations exceeded to a maximum of 2000. The convergence rate of the IE-FFT with CFIE bounds on a small number of iterations.

A realistic example considered here is a generic battleship. When the incident wave at $\theta = 90^{\circ}$ and $\phi = 0^{\circ}$ is considered, the bistatic RCS of $\theta\theta$-polarization is computed by the IE-FFT algorithm with CFIE without the help of any preconditioner. The discretization of the triangular mesh is 5 elements per wavelength. Third-order Lagrange polynomials are used to interpolate free-space Green's function. The results of bistatic RCS at a frequency of 30 MHz are shown in Fig. 4. The results of the IE-FFT with CFIE are compared with those of the EFIE by the traditional MoM. Both results have very good agreements.

Figure 5 shows the results of bistatic RCS at a frequency of 60 MHz. Due to the prohibitive complexity of the conventional MoM, we compare the results of the CFIE for the IE-FFT with those of the EFIE for the ACA algorithm [5]. Both results have very good agreements.

The results of bistatic RCS at a frequency of 120 MHz are shown in Fig. 6. The results between the IE-FFT of the EFIE and the IE-FFT with CFIE are compared. Both results have reasonable agreements.

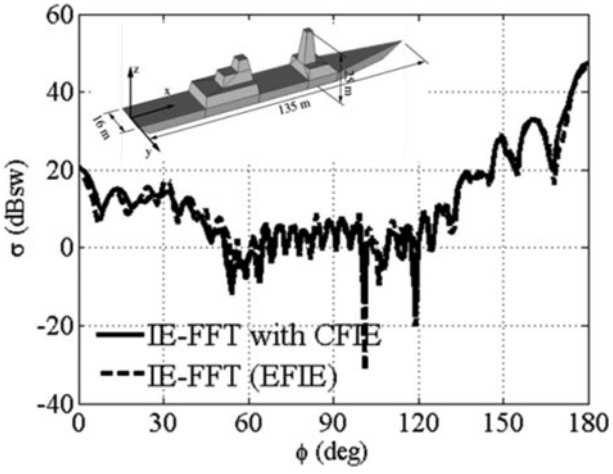



**Fig. 6.** Comparison of the bistatic RCS results for the battleship at 120 MHz ($\theta\theta$-polarization) using the IE-FFT with CFIE and EFIE.

All the numerical complexities of the performed simulations are tabularized. First, the IE-FFT algorithm with CFIE is compared with the traditional MoM with EFIE in Table 3.

The number of unknown is 12 972 and the operating frequency is 30 MHz. The CPU time of the MVM per iteration and the number of iterations are shown in the first and second columns. The memory of $Z^{corr}$ and $\mathbf{\Pi}$ matrices and $G$ matrix is

https://doi.org/10.1017/S1759078720000653 Published online by Cambridge University Press

**Table 3.** Numerical complexities between the IE-FFT with CFIE and the traditional MoM of the EFIE for the battleship at 30 MHz (The number of unknowns is 12 972)

| | MXV/iteration (s) | Number of iterations | MoM (MB) | Preconditioner (MB) |
|---|---|---|---|---|
| MoM (EFIE) | 2.80 | 104 | 673 | 34 |
| IE-FFT (CFIE) | 0.91 | 90 | 69 ($Z^{corr}+\Pi$)<br>4 ($G$) | – |

**Table 4.** Numerical complexities between the CFIE-FFT and the ACA of the EFIE for the battleship at 60 MHz (the number of unknowns is 48 363)

| | MVM/iteration (s) | Number of iterations | MoM (MB) | Preconditioner (MB) |
|---|---|---|---|---|
| ACA (EFIE) | 2.92 | 104 | 697 | 234 |
| IE-FFT (CFIE) | 6.22 | 89 | 250 ($Z^{corr}+\Pi$)<br>33 ($G$) | – |

**Table 5.** Numerical complexities between the IE-FFT with CFIE and the IE-FFT with EFIE for the battleship at 120 MHz (the number of unknowns is 189 606)

| | MVM/iteration (s) | Number of iterations | MoM (MB) | Preconditioner (MB) |
|---|---|---|---|---|
| IE-FFT (EFIE) | 26.63 | 166 | 422 ($Z^{corr}+\Pi$)<br>268 ($G$) | 355 |
| IE-FFT (CFIE) | 46.36 | 80 | 974 ($Z^{corr}+\Pi$)<br>268 ($G$) | – |

**Table 6.** The number of iterations with GMRES method according to the weighting constant of the IE-FFT with CFIE for the battleship at 60 MHz (the number of unknowns is 48 363)

| $\rho$ | 0 | 0.1 | 0.3 | 0.5 | 0.7 | 0.9 | 1 |
|---|---|---|---|---|---|---|---|
| Number of iterations | >5000 | 129 | 26 | 30 | 51 | 136 | >5000 |

compared with that of the traditional MoM matrix in the third column. The traditional MoM requires an extra memory of geo-neighboring preconditioner [15] in the fourth column. It is undoubtedly proven that the IE-FFT with CFIE is more efficient than the traditional MoM. Second, the IE-FFT with CFIE is compared with the ACA of the EFIE in Table 4.

The number of unknowns is 48 363 and the operating frequency is 60 MHz. Because of the memory limit of the current processor, the simulation cannot be operated by the conventional MoM. Even though the matrix of the IE-FFT with CFIE is non-symmetric, the memory of the IE-FFT with CFIE is approximately three times smaller than that of the ACA. The MVM per iteration of the IE-FFT with CFIE is twice worse than that of ACA. However, the ACA does not converge without the geo-neighboring preconditioner. Finally, the IE-FFT with CFIE is compared with the IE-FFT of the EFIE in Table 5.

Due to the storage limit of the processor in the simulation, the ACA cannot be performed. The number of unknowns is 189 606 and the operating frequency is 120 MHz. The total CPU time of both methods is approximately similar. The total storage of the IE-FFT looks better than that of the IE-FFT with CFIE. Nevertheless, the memory of the preconditioner is the only final result except for extra memory of reordering, factorization, etc. The realistic memory of the preconditioner is much bigger than the final written result. In the simulation, the IE-FFT of the EFIE does not converge without the geo-neighboring preconditioner. From the tables, the memory of $Z^{corr}$ and $\mathbf{\Pi}$ matrices

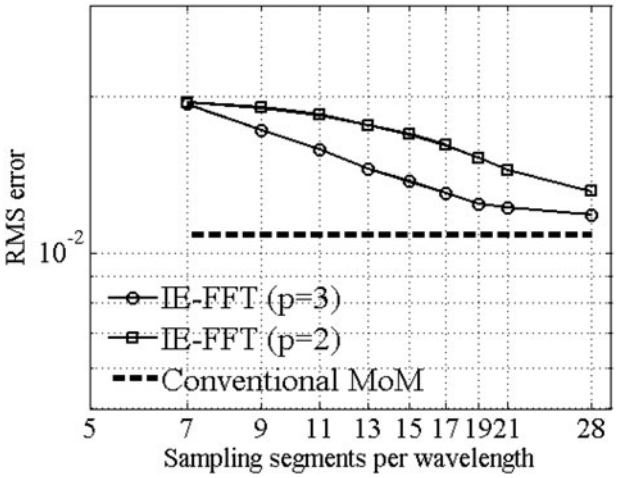



**Fig. 7.** The RMS errors of the bistatic RCS calculations versus the sampling segments per wavelength ($p = 2, 3$).

follows $O(N)$ complexity. The coefficient matrix of the free-space Green's function $G$ is $O(N^{1.5})$ complexity. Therefore, the coefficient matrix will be more dominant as the electrical length is larger. Table 6 shows the number of iterations of the GMRES method according to the weight constant $\rho$ of the IE-FFT with CFIE at a frequency of 60 MHz.

https://doi.org/10.1017/S1759078720000653 Published online by Cambridge University Press

Both the EFIE and MFIE formulations accelerated by the IE-FFT do not converge within the number of iterations exceeded to a maximum of 5000. Both formulations may have internal resonance for this specific case. However, the IE-FFT with CFIE is free of internal resonance and has reliable convergence rate and solution.

In Fig. 7, the study of the error control of the IE-FFT with CFIE is performed indirectly in terms of the RMS errors of the bistatic RCS calculations [2]. The numerical simulations from the sampling segments per wavelength are carried out for 1 m PEC sphere at a frequency of 600 MHz. The average RMS errors are plotted. The dashed line indicates the RMS error of the conventional MoM with EFIE. The solid line with circular markers and dash-dotted line with square markers represent the RMS errors of the IE-FFT for the second- and third-order Lagrange polynomials, respectively. The RMS errors of the IE-FFT with CFIE converge to those of the conventional MoM as the sampling segments increase.

## Conclusion

The IE-FFT algorithm with CFIE has been implemented and demonstrated for arbitrary-shaped 3-D PEC objects. In the PEC sphere example, the IE-FFT algorithm with CFIE is shown to achieve $O(N^{1.5})$ and $O(N^{1.5}\log N)$ complexities for memory and MVM per iteration, respectively. The realistic example of the generic battleship shows the reliability of the IE-FFT algorithm with CFIE. The IE-FFT with CFIE is free of internal resonance and has reliable convergence rate and solution. The IE-FFT algorithm with CFIE can handle up to approximately 0.3 million unknowns with only 2GB memory.

## References


1. **Harrington RF** (1968) *Field Computation by Moment Methods*. New York, USA: The Macmillan Company.
2. **Seo SM, Wang C and Lee JF** (2009) Analyzing PEC scattering structure using an IE-FFT algorithm. *Applied Computational Electromagnetics Society Journal* **24**, 116–128.
3. **Song JM and Chew WC** (1995) Multilevel fast multipole algorithm for solving combined field integral equation of electromagnetic scattering. *Microwave and Optical Technology Letters* **10**, 14–19.
4. **Seo SM and Lee J-F** (2004) A single-level low rank IE-QR algorithm for PEC scattering problems using EFIE formulation. *IEEE Transactions on Antennas and Propagation* **52**, 2141–2146.
5. **Zhao K, Vouvakis MN and Lee J-F** (2005) The adaptive cross approximation algorithm for accelerated method of moments computations of EMC problems. *IEEE Transactions on Electromagnetic Compatibility* **47**, 763–773.
6. **Bleszynski E, Bleszynski M and Jaroszewicz T** (1996) AIM: adaptive integral method for solving large-scale electromagnetic scattering and radiation problems. *Radio Science* **31**, 1225–1251.
7. **Phillips JR and White JK** (1997) Precorrected-FFT method for electrostatic analysis of complicated 3-D structures. *IEEE Transactions on Computer-Aided Design of Integrated Circuits and Systems* **16**, 1059–1072.
8. **Nie XC, Li L and Yuan N** (2002) Precorrected-FFT algorithm for solving combined field integral equation applied to electrically large objects. *Journal of Electromagnetic Waves* **16**, 1171–1187.
9. **Seo SM and Lee JF** (2005) A fast IE-FFT algorithm for solving PEC scattering problem. *IEEE Transactions on Magnetics* **41**, 1476–1147.
10. **An X and Lü Z-Q** (2008) Application of IE-FFT with combined field integral equation to electrically large scattering problems. *Microwave and Optical Technology Letters* **50**, 2561–2566.
11. **Xie J-Y, Zhou H-X, Li W-D and Hong W** (2012) IE-FFT for the combined field integral equation applied to electrically large objects. *Microwave and Optical Technology Letters* **54**, 891–896.
12. **Rao SM, Wilton DR and Glisson AW** (1982) Electromagnetic scattering by surfaces of arbitrary shape. *IEEE Transactions on Antennas and Propagation* **30**, 409–418.
13. **Vico F, Greengard L and Ferrando M** (2106) Fast convolution with free-space Green's functions. *Journal of Computational Physics* **323**, 191–203.
14. **Golub GH and Van Loan CF** (1996) *Matrix Computations*. Baltimore and London: The Johns Hopkins University Press.
15. **Lee JF, Lee R and Burkholder RJ** (2003) Loop star basis functions and a robust preconditioner for EFIE scattering problems. *IEEE Transactions on Antennas and Propagation* **51**, 1855–1863.




**Seung Mo Seo** received the B.S. degree from Hong-Ik University in 1998 and the M. S. and Ph.D. degrees from The Ohio State University in 2001 and 2006, respectively, all in Electrical Engineering. During 2007–2010, he stayed in DMC R&D Center, Samsung Electronics. He is now with Agency for Defense Development.

https://doi.org/10.1017/S1759078720000653 Published online by Cambridge University Press